Stable and selective syngas production from dry CH_4-CO_2 streams over supported bimetallic transition metal catalysts

Petar Djinović*, Albin Pintar

Department for Environmental Sciences and Engineering, National Institute of Chemistry, Hajdrihova 19, SI-1000 Ljubljana, Slovenia

ABSTRACT

Syngas production from CH_4 and CO_2 was investigated over bimetallic nickel-cobalt catalysts, promoted by a $CeZrO_2$ redox component. The appropriate design of active sites responsible for methane and CO_2 activation (bimetallic clusters below 45 nm, adjacent to oxygen vacancy sites of the $CeZrO_2$ solid solution) enabled kinetic balancing of both reaction halves, producing catalysts that are highly resistant to carbon accumulation in a wide range of CH_4-CO_2 feed compositions. With the employed approach, carbon accumulation can be prevented over metal clusters that are 2-fold larger compared to state-of-the-art. By anchoring the active NiCo bimetallic and $CeZrO_2$ redox components over a high surface area β-SiC carrier (3NiCo/CeZrO2/S catalyst), the redox promoter is diluted and sintering of bimetallic NiCo clusters is reduced. At ambient pressure, a remarkably stable catalytic performance for 550 h was recorded with a produced H_2/CO ratio of 0.82, methane reforming rate of 0.18 mol/g_{cat} h and negligible carbon accumulation. Stable operation is maintained for 60 h during reforming at 20 bar, producing syngas with a H_2/CO ratio of 0.33. Importantly, accumulated carbon yield is 2–3 orders of magnitude lower compared to state-of-the-art. These results constitute a promising basis for the design of a prospective technology for CO-rich syngas production through CH_4-CO_2 reforming.

© 2017 Elsevier B.V. All rights reserved.

1. Introduction

Global syngas production accumulated to 116 GWth in 2014 and is projected to reach 213 GWth by 2020 [1]. The indirect conversion of natural gas into higher value chemicals and fuels via syngas (mixture of H_2 and CO) is superior with regard to efficiency compared to direct conversion technologies (e.g. methane oxidative coupling) and remains the prevailing industrial route. Typically, the syngas production process is selected by the H_2/CO ratio requirements of the downstream synthesis process. For example, direct dimethyl ether synthesis [2], high-temperature Fischer-Tropsch [3] and acetic acid synthesis [4] require CO rich syngas that is not produced by established syngas technologies like steam methane reforming [4]. As a result, CO_2 reforming of methane, also known as dry reforming (DRM), is an attractive alternative for production of CO-rich syngas. Reactants required for this reaction can originate either from vast reserves of natural gas or abundant sources of biogas. Global biogas production, which represents a renewable

alternative to fossil sourced methane, is growing rapidly [5]. With the addition of CO_2, for example CO_2-rich flue-gas streams from ammonia plants, the CH_4-CO_2 ratio in the feed can be modified. The absence of steam in the feed results in CO rich syngas (H_2/CO < 1) and circumvents the required energy input for steam generation. However, it also substantially increases the thermodynamic driving force for carbon formation on the catalyst's surface, which leads to a fast increase in pressure drop across the catalyst bed and prevents stable long-term operation.

During high pressure CH_4-CO_2 reforming, the coke formation rate increases noticeably, which makes the catalyst and reactor design significantly more complicated and has to date represented a formidable obstacle. However, high pressure reforming is the industrially favored route, because cooling and re-compression of syngas for downstream processes (for instance, methanol synthesis is carried out at ∼50 bar, Fischer-Tropsch synthesis at ∼20 bar) substantially lower the overall process efficiency.

In a recent work, Vasiliades et al. [6] synthesized a series of 5 wt.% Ni-CePrO2-δ catalysts and through advanced fundamental investigations examined the role of the redox property of support and the influence of support's chemical composition (Ce/Pr ratio) on the concentration of active and inactive carbon species and their
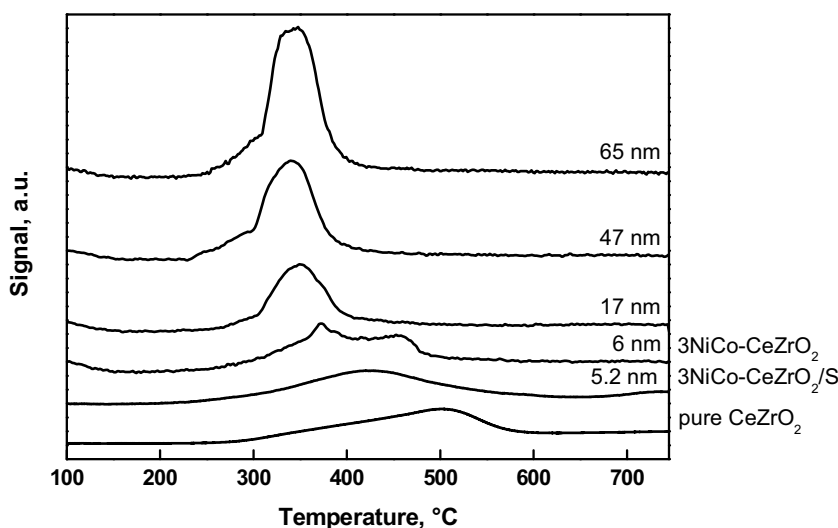
Fig. 1. H$_2$-TPR profiles of the NiCo/CeZrO$_2$ catalysts containing bimetallic NiCo clusters of various sizes. NiCo clusters were deposited over CeZrO$_2$ support with high oxygen mobility (67% Ce$^{4+} \rightarrow$ Ce^{3+} reduction achieved during the employed reduction protocol).

origin (CH$_4$ vs. CO$_2$ molecular route). Inactive carbon was mainly responsible for the catalyst deactivation.

In this work, a multifunctional approach to catalyst design is presented. A bifunctional pathway with concerted action of metal and support is required for balanced CH$_4$ and CO$_2$ activation [7,8]. This yields active and stable supported transition metal catalysts for CH$_4$-CO$_2$ reforming reaction both at ambient and elevated pressures over extended time periods.

A thermally stable carrier (β-SiC) provided both structural support and spatial segregation of nickel-cobalt bimetallic nanoclusters and CeZrO$_2$ redox promoter. Nickel was alloyed with cobalt in order to modify its electronic structure and moderate their activity in methane activation [9,10]. Alloying nickel with cobalt breaks the integrity of surface nickel ensembles [11,12], which decreases the apparent nickel particle size, resulting in considerable suppression in the growth of carbon nanotubes that is strongly size dependent [13,14]. Redox functionality was provided by nanocrystalline CeZrO$_2$ solid solution [15], that continuously generates (by CO$_2$ disproportionation) [8,16], and supplies active oxygen species, which spill over to the neighboring transition metal clusters and continuously gasify the formed carbon precursors and deposits [17,18].

2. Experimental

The 3NiCo/CeZrO$_2$ catalyst (3 wt.% NiCo, Ni:Co = 40:60, CeO$_2$:ZrO$_2$ = 80:20, w/w) was synthesized according to the procedure described by Djinović et al. [17]. Variation of NiCo bimetallic cluster size was achieved by progressively increasing the metal content from 3 to 6, 12 and 18 wt.%, respectively. Deposition precipitation technique with urea as the precipitating agent was used to produce a 3NiCo-CeZrO$_2$/S catalyst (containing 50 wt.% β-SiC, grains between 40 and 150 μm, SICAT, Germany, S$_{BET}$ = 17 m^2/g, V$_{tot}$ = 0.07 cm^3/g, D$_{av}$ = 17 nm). During deposition, β-SiC was dispersed in ultrapure water. Cerium, zirconyl, nickel and cobalt nitrate precursors were added in an amount to result in 47 wt.% CeZrO$_2$ and 3 wt.% NiCo in the final catalyst. The precipitation was allowed to take place for 22 h under stirring at 90 °C. The precipitate was filtered, washed, dried at 100 °C for 6 h and calcined in air for 12 h at 800 °C.

Active metal dispersion was measured using the H$_2$ chemisorption-TPD technique (AutoChem II 2920 apparatus, Micromeritics). During analysis, 100 mg of sample was positioned

in the U-shaped quartz tube and reduced in 5% H$_2$/Ar mixture at 750 °C for 1 h. The sample was cooled to 30 °C, saturated with 5% H$_2$/Ar for 20 min and degassed in Ar for 1 h to desorb weakly bound H$_2$. TPD experiment was performed from 30 to 800 °C. Active metal cluster size was calculated from the dispersion [19], based on the low-temperature H$_2$ desorption peak area assuming Ni-H and Co-H stoichiometry equal to 1.

The amount of labile oxygen species in CeZrO$_2$ mixed oxide was determined using the H$_2$-TPR technique (AutoChem II 2920 apparatus). During the experiment, 100 mg of sample was positioned inside the quartz tube and pretreated in 10% O$_2$/He at 500 °C for 20 min. After sample cooling to 50 °C, it was degassed in Ar for 30 min. TPR analysis was performed between 100 and 750 °C, using 25 mL/min of 5% H$_2$/Ar and a heating rate of 10 °C/min.

TEM-EDXS examinations were conducted using a JEOL ARM 200 CF scanning transmission electron microscope, equipped with a cold field-emission gun, probe spherical aberration corrector (CESCOR unit from CEOS, Germany) and Jeol Centurio EDXS system with 100 mm^2 SDD detector. Specimens were ultrasonically dispersed in ethanol and deposited on a copper grid covered with a carbon film prior to analysis.

Catalytic tests were performed in a Microactivity Reference reactor system (PID Eng&Tech) at 750 °C. For the tests performed at 1.2 bar, 500 mg of catalyst was diluted 6 fold with SiC (grain size of 200–500 μm) to form the catalytic bed, sandwiched between two flocks of quartz wool and positioned in the tubular quartz reactor (I.D.=10 mm). The catalyst was reduced in situ at 750 °C for 1 h in a 20% H$_2$/N$_2$ stream. A mixture of CH$_4$ and CO$_2$ (50 NmL/min each) was fed into the reactor (WHSV = 12 L/(g$_{cat}$h)). During experiments at 20 bar, 50 mg of catalyst was diluted with SiC (as described above) and fixed between two quartz wool flocks. The feed gas consisted of CH$_4$ and CO$_2$ (25 NmL/min each), WHSV = 60 L/(g$_{cat}$h). The reaction was performed in a quartz tube (I.D.=6 mm), which was tightly fitted inside a tubular reactor made of AISI316 stainless steel (Autoclave Engineers). At both ends, Teflon O-rings were used to prevent gas bypassing the catalytic layer. Reactor volume before and after the catalytic bed was filled with SiC sand in order to minimize the contribution of homogeneous gas-phase reactions. Temperature was measured using a K-type thermocouple that was placed just above the catalytic bed. Blank tests revealed negligible contribution of the reactor to methane conversion (below 1% at 750 °C and 20 bar). Gases discharged from the reactor were analyzed by gas chromatography (Agilent 7890A equipped with Poraplot Q and
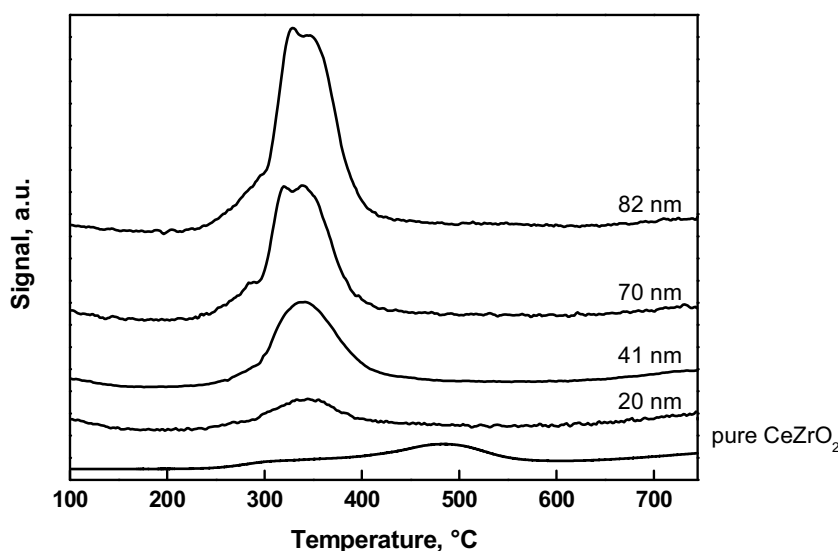
Fig. 2. H$_2$-TPR profiles of the NiCo/CeZrO$_2$ catalysts containing NiCo bimetallic clusters of various sizes. NiCo clusters were deposited over CeZrO$_2$ support with intermediate oxygen mobility (51% Ce^{4+} → Ce^{3+} reduction during the employed reduction protocol).
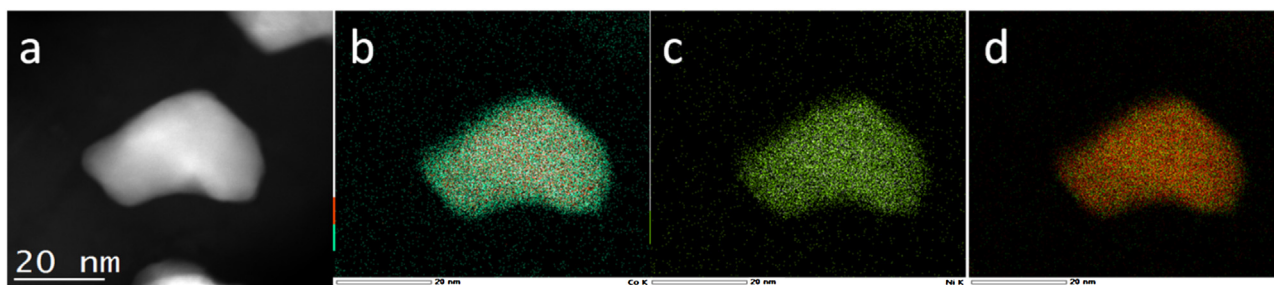

Fig. 3. a) HAADF/STEM micrograph of the NiCo bimetallic cluster in the fresh 3NiCo/CeZrO$_2$ catalyst, b) EDXS elemental map of Co K edge, c) Ni K edge and d) their overlay. Ideal matching of the Ni and Co maps strongly suggests presence of homogeneous, alloyed NiCo bimetallic clusters.

Molesieve 5A columns). Carbon amounts accumulated during catalytic tests were measured using a CHNS elemental analyzer (model 2400 by Perkin Elmer).

3. Results and discussion

H$_2$-TPR analysis was used for evaluating the amount of labile oxygen in the NiCo-CeZrO$_2$ catalysts. The fraction of Ce^{4+} → Ce^{3+} reduction in tested catalyst groups was 67% and 51%, respectively and changed only slightly (up to 2%) after metal addition. Oxygen mobility of the CeZrO$_2$ mixed oxides depends primarily on efficient substitution of Ce with smaller Zr ions, which can be successfully realized with the appropriate synthesis technique and redox treatment [15,20].

As can be seen from the results in Figs. 1 and 2, the recorded TPR profiles depend strongly on the size of NiCo clusters. The reduction of catalysts containing smallest NiCo clusters (5.2 and 6 nm on average, Fig. 2) occurs as a broad feature between 250 and 550 °C. Based on the high temperature required for the reduction, oxygen appears to be most strongly bound in the smallest NiCo clusters. With increasing average size of the NiCo cluster, the reduction peak shifts towards lower temperatures, exhibiting a maximum at 340 °C. The shift is connected to the decreasing of the interface between the NiCo bimetallic and CeZrO$_2$ redox components. The intensity of the reduction peak is related to the amount of reducible phases in the analyzed material and increases with increasing NiCo content from 3 to 18 wt.% in the catalysts. The amount of consumed H$_2$ dur-

ing the analyses greatly surpassed the theoretical amount required for complete reduction of NiO and Co$_3$O$_4$ to their metallic form, confirming concurrent reduction of the CeZrO$_2$ redox support. The alloying of Ni and Co and formation of NiCo bimetallic clusters in the catalysts was confirmed by TEM-EDXS analysis (Fig. 3).

Fig. 4a shows dependence of carbon yield over the bimetallic NiCo/CeZrO$_2$ catalysts as a function of metal cluster size ranging from 6 to 80 nm during the methane dry reforming reaction. The results are presented for three groups of catalysts that differ in the amount of labile oxygen in the CeZrO$_2$ support (32–42, 51 and 67%). When NiCo clusters are below 10 nm in size, the tendency for carbon accumulation is low and loosely influenced by the amount of labile oxygen of the CeZrO$_2$ support (green squares). Carbon yield is high over materials with the NiCo cluster size ranging between 20 and 85 nm when employing a CeZrO$_2$ support with intermediate oxygen mobility (black squares).

Over CeZrO$_2$ support with high oxygen mobility (red squares), very low carbon accumulation can be maintained over NiCo bimetallic clusters which are below 20 nm in size. With an increase of average NiCo cluster size above 45 nm, carbon accumulation drastically increases and is again not influenced by the amount of labile oxygen of the CeZrO$_2$ support.

The main advantage of the redox promoted NiCo catalyst is that the bimetallic clusters can be considerably (up to 4 fold) larger (45 nm) compared to values mentioned in the literature (7–10 nm [21–23]), yet the catalyst is not prone to coking. Briefly, to ensure low carbon yields over the catalyst during the CH$_4$-CO$_2$ reforming
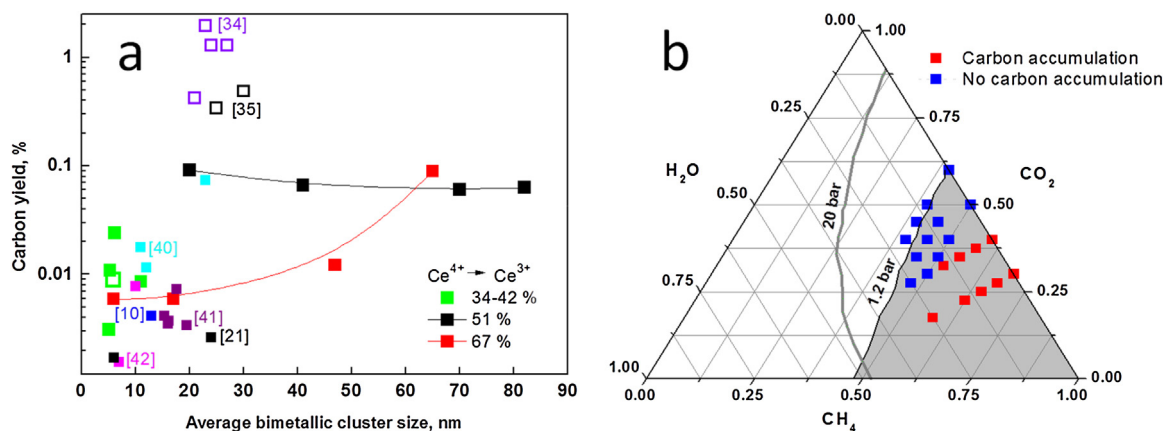
Fig. 4. a) Carbon yield dependency on average nickel-cobalt bimetallic cluster size for three groups of $NiCo/CeZrO_2$ catalysts exhibiting different degrees of labile oxygen in $CeZrO_2$ support. Carbon yield is calculated as: (moles of carbon accumulated on the catalyst during the reaction/moles of CH_4 and CO_2 fed during the reaction) × 100%). Promising nickel based catalytic formulations during CH_4-CO_2 reforming reaction with equimolar CH_4/CO_2 ratio, T = 750 °C, WHSV = 48–180 L/(g_cat h) and P = 1 bar, are shown for comparison [10,21,40–42]. Empty symbols represent carbon yields at 20 bar [34,35]. b) Ternary phase diagram of CH_4, CO_2 and H_2O feed composition with regions forecasting coke formation, calculated for T = 750 °C and p = 1.2 and 20 bar. The calculations are based on free Gibbs energy minimization using Gaseq software. Individual experiments with $3NiCo/CeZrO_2$ catalyst, presented by red and blue squares were performed at T = 750 °C, TOS = 10 h, WHSV = 60 L/(g_cat h) and p = 1.2 bar. (For interpretation of the references to colour in this figure legend, the reader is referred to the web version of this article.)
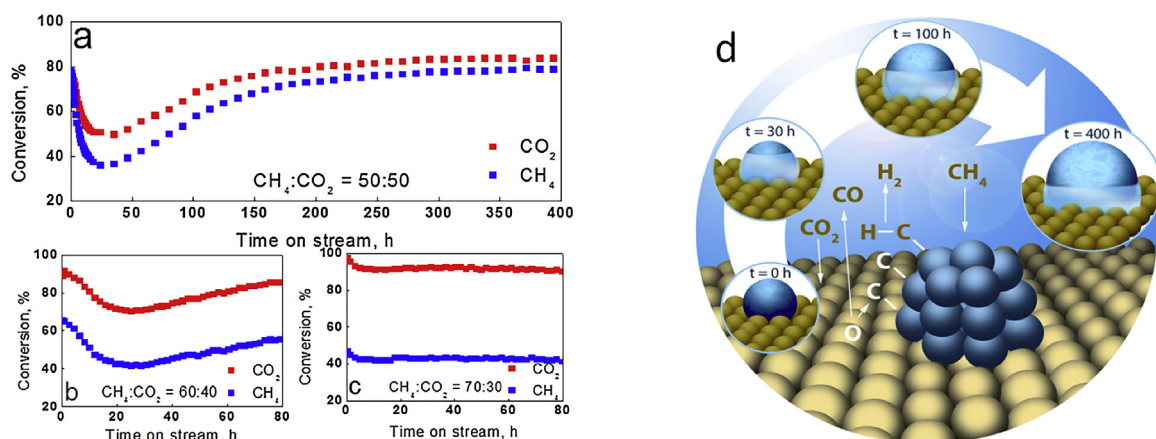

Fig. 5. Conversion of CH_4 and CO_2 for the $3NiCo/CeZrO_2$ catalyst as a function of TOS for progressively CO_2-leaner feed streams (5a–c). Evolution of catalyst's working state as a function of time on stream (5d).

reaction using equimolar ratio of both reactants, bimetallic NiCo clusters below 45 nm and $CeZrO_2$ with high extent labile oxygen have to be simultaneously present.

In Fig. 4b, the ternary phase diagram of CH_4, CO_2 and H_2O feed composition is presented. It is divided into two regions where, accordingly to thermodynamic calculations based on Gibbs free energy minimization, coke formation either is, or is not foreseen. The role of carbon scavenging by the oxygen species (supplied by the $CeZrO_2$ phase) is clearly presented, as the safe range of operating conditions (where no carbon was accumulated over the catalyst during reaction) can be noticeably extended towards methane rich feed compositions (blue symbols in Fig. 4b). This is important as it overcomes the need for feeding substantial surplus of oxidant (O_2 and especially H_2O), which is the established practice in industrial methane reforming processes [24].

In order to assure high H_2 selectivity and at the same time low carbon yield, one has to precisely tailor the catalyst composition and morphology in order to kinetically balance steps of CH_4 activation occurring over NiCo bimetallic clusters [7,8], on one hand and CO_2 activation predominantly at the surface oxygen vacancy sites of the $CeZrO_2$ support [7,8,16], on the other.

CO_2 acts as a source of oxygen species, which by combining with carbon species (accumulating on the bimetallic clusters) generate

CO and complete the catalytic cycle. Oxygen transfer along the surface of doped CeO_2 supports was identified as very fast using isotopically labeled $^{18}CO_2$ and SSITKA technique [7], however, not selective for carbon oxidation only and can: (i) oxidize hydrogen species located at the proximity of the metal-support interface to form water. This exhibits itself as lower H_2 selectivity [25]. In addition, oxygen spillover to the NiCo bimetallic clusters can also have a detrimental effect, namely reversible catalyst deactivation by oxidation.

A macroscopic dynamic catalyst behavior is depicted in Fig. 5a for the $3NiCo/CeZrO_2$ catalyst as a function of time on stream (3 wt.% NiCo loading, average NiCo cluster size 6 nm, 67% of removable oxygen in $CeZrO_2$ redox support, equimolar CH_4 and CO_2 feed ratio).

The initial stage of reaction (30 h TOS) is characterized by fast deactivation, which is followed by slow reactivation. The origin of deactivation was identified indirectly using progressively CO_2 leaner feed compositions [26]. CO_2 disproportionation over the bimetallic NiCo clusters is not likely the predominant source of catalyst deactivation due to its inability to maintain the nickel in the oxidized state at the employed reaction temperature of 750 °C [27]. Instead, lower concentration of CO_2 in the feed results in less oxygen species being supplied to the NiCo bimetallic clusters. This
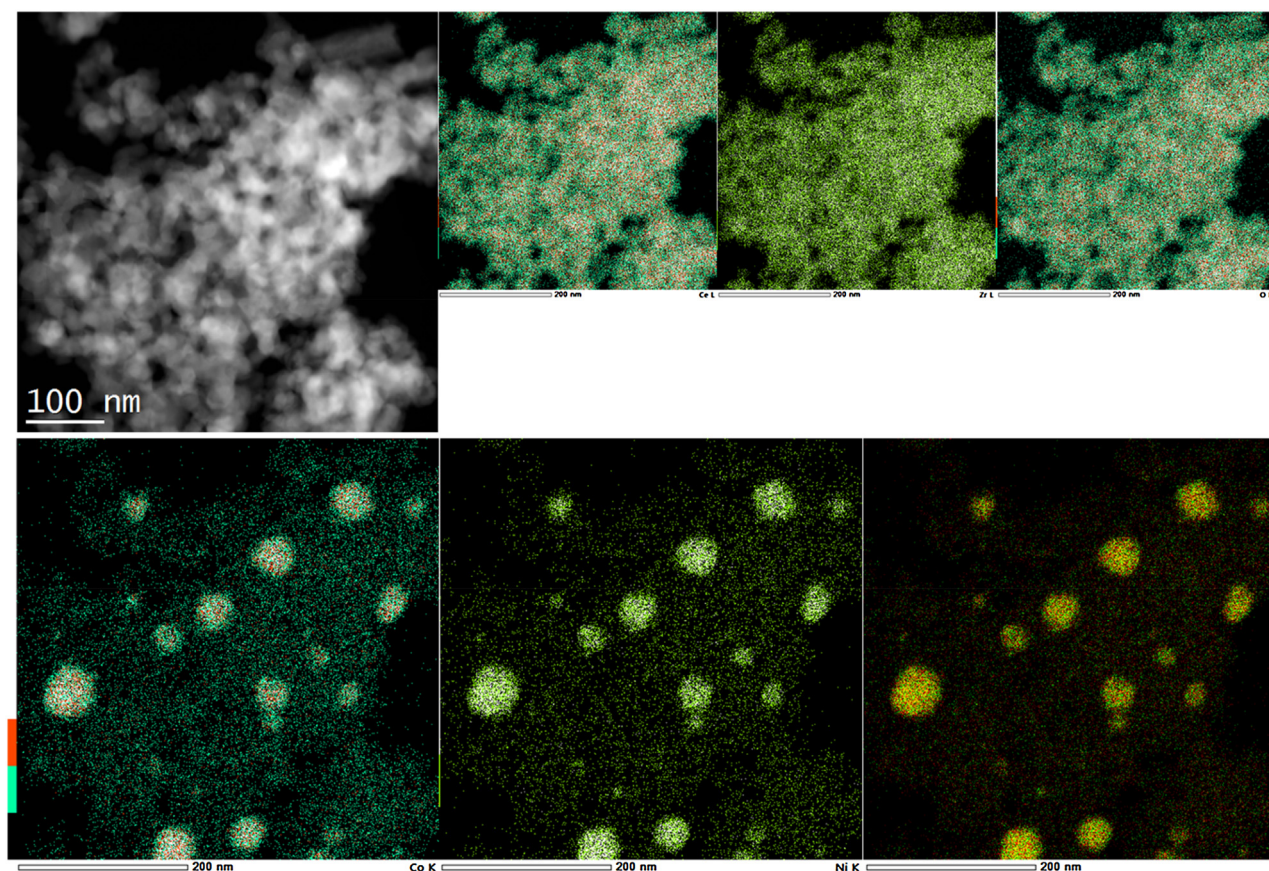
Fig. 6. HAADF/STEM micrograph of the 3NiCo/CeZrO$_2$ catalyst after 400 h TOS (top left) with corresponding EDXS elemental mapping. Upper row from left to right: Ce L edge, Zr L edge and O K edge. Lower row from left to right: Co K edge, Ni K edge and their overlay. Ideal matching of the Ni and Co maps strongly suggests presence of homogeneous alloyed NiCo bimetallic clusters.

results in a lower extent of NiCo bimetallic cluster oxidation and less water produced during the reaction (highest measured concentrations were 9.8, 4.6 and 0.7 vol.% when CH$_4$:CO$_2$ feed ratio was incrementally changed from 50:50 to 60:40 and finally to 70:30). The decrease in CH$_4$ conversion was more pronounced compared to the drop of CO$_2$ conversion. Also, by having in mind that CH$_4$ activation takes place over bimetallic clusters [7,8], it is likely that deactivation (oxidation) of NiCo bimetallic component occurred. The observed deactivation was accompanied by a drop in produced H$_2$ and CO. On the other hand, H$_2$O production was improved during the deactivation (Electronic Supplementary Information, Figs. S1–S3), which is consistent with the catalytic behavior of oxidized Ni and Ru catalysts in the methane dry reforming reaction [7]. As can be seen in Fig. 5b and c, deactivation can be minimized or completely avoided with CO$_2$ leaner feed streams. When 10 vol.% water is co-fed, the extent of deactivation is higher (Fig. S4), clearly indicating water as the main source of observed catalytic behavior.

The regeneration rate of catalyst's activity is significantly slower and is governed by sintering of CeZrO$_2$ support and growth of NiCo clusters. This was tested with a series of three chemically identical catalysts (3NiCo/CeZrO$_2$), calcined at progressively higher temperature (650, 750 and 850 °C), resulting in increasingly sintered morphology (Electronic Supplementary Information, Table S1).

It was anticipated that more heavily sintered catalyst samples will, under the applied reforming conditions (T = 750 °C, P = 1.2 bar, CH$_4$:CO$_2$ = 1:1), reach the stable state in a shorter time. Indeed, quasi steady-state performance was achieved at progressively shorter times, namely 250 (Fig. 5a), 150 and 100 h TOS, respectively. The evolution of the catalyst's state as a function of time on stream is schematically shown in Fig. 5d. The active NiCo bimetallic clusters

measure on average 6 nm in size and are metallic at TOS = 0 h. In the initial 30 h of reaction, the metal clusters grow as a result of sintering to 18.5 nm. Due to a large metal-support interface, the oxygen spillover from the support causes their partial oxidation, resulting in a substantial deactivation. During the course of reaction, sintering of the metal clusters continues and the metal-support perimeter continuously decreases (TOS = 100 h). As a result, less oxygen can be supplied to the metal clusters and their oxidized fraction decreases. This manifests itself as slow regeneration of catalytic activity. At 400 h TOS, bimetallic clusters have grown to 46 nm, as was identified using H$_2$-TPD and visualized by TEM-EDX (Fig. 6). The oxidized part of the metal clusters is low and the quasi steady state is achieved. The way the coalescence (sintering) of metal particles takes place and how this influences metal-support perimeter (or length of metal particle-support circumference, expressed in cm/g of active metal) is not straightforward [28,29]. It will depend on the metal particle size distribution and the rate of coalescence taking place for a given supported metal catalytic system.

Extremely low carbon yield (8.9 × 10^{-5}%) was observed over the 3NiCo/CeZrO$_2$ sample after the 400 h catalytic test, which provides solid evidence of kinetically balanced reaction steps on the catalyst surface.

Ni particles, larger than 45 nm, supported over CePrO$_{2-\delta}$ mixed oxides were very recently identified with very low inactive carbon content accumulated during 25 h TOS. On the other hand, absence of Pr^{3+} dopant which stimulates the formation of oxygen vacancies in CeO$_2$, caused a strong increase of carbon deposits [6]. The present results and those reported by Vasiliades et al. [6], demonstrate that the rate of carbon accumulation is the net result of many processes that form and consume inactive carbon, and that participation of
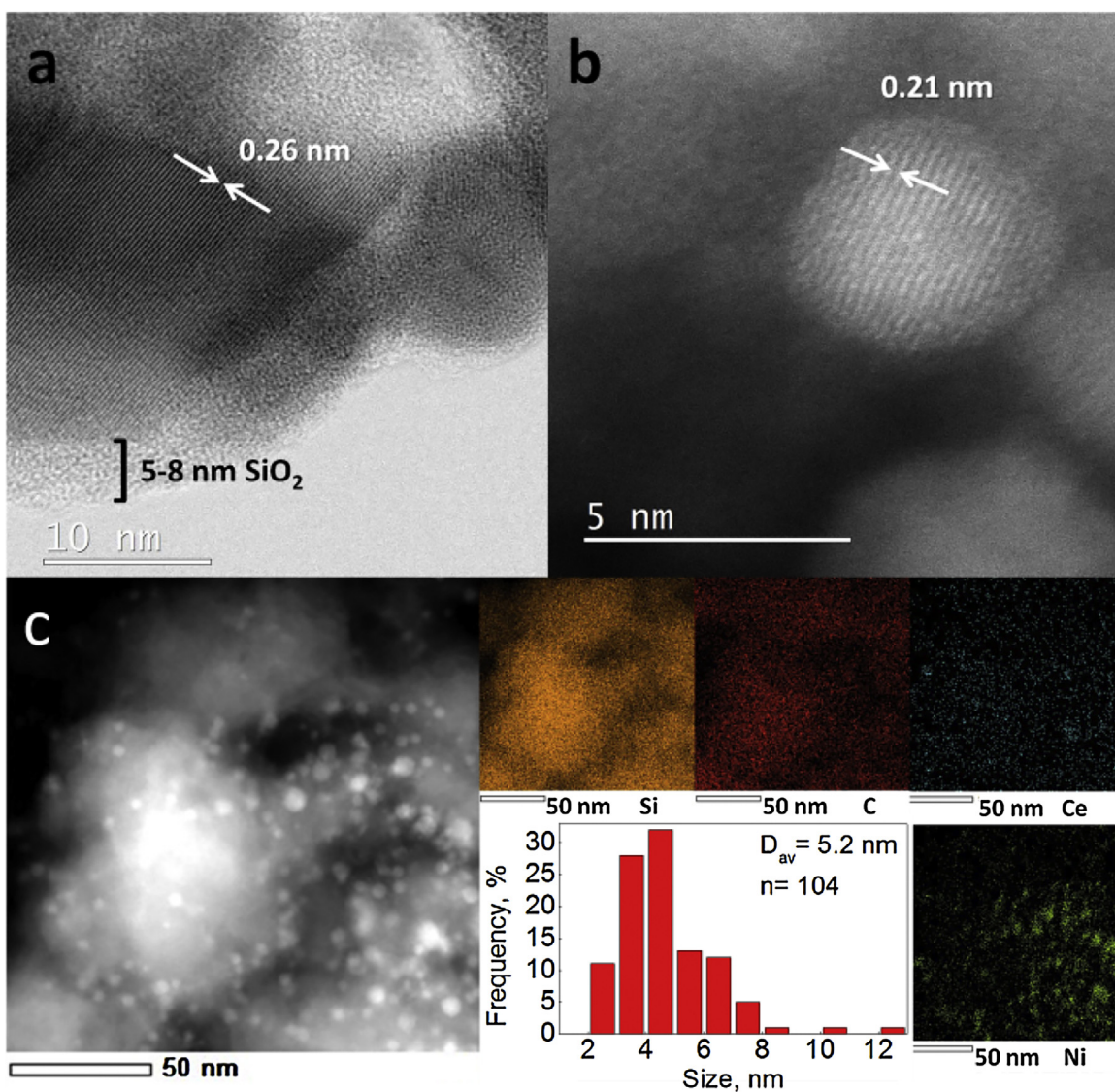
Fig. 7. TEM images of 3NiCo-CeZrO$_2$/S catalyst: a) β-SiC covered with an amorphous SiO$_2$ layer, 5–8 nm thick, b) HRTEM image of the NiCo bimetallic cluster viewed along the Ni [100], lattice plane and c) ADF-STEM image of the catalyst (brighter spots represent NiCo clusters) with corresponding EDXS elemental maps and NiCo cluster size distribution.
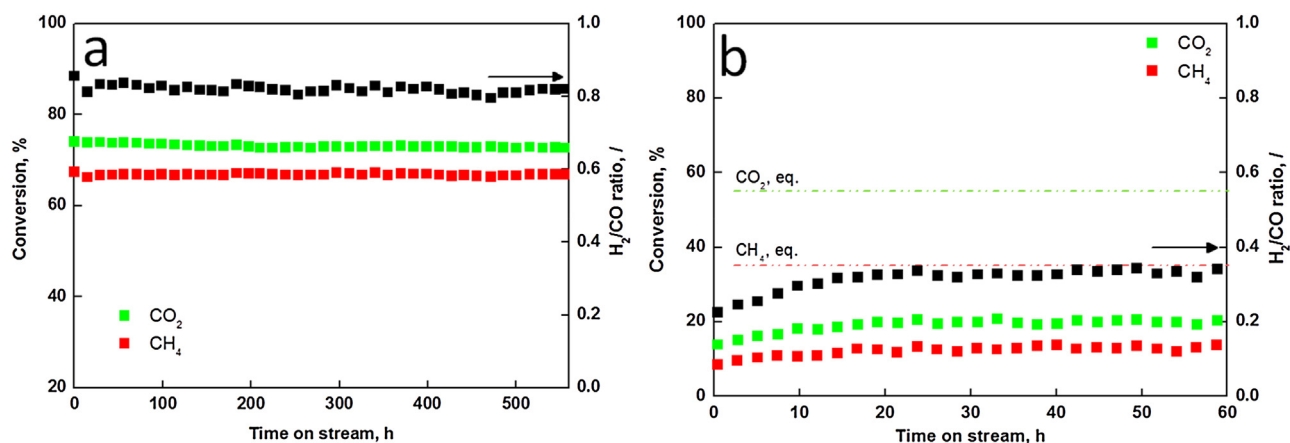

Fig. 8. CH$_4$ and CO$_2$ conversion as well as H$_2$/CO ratio produced over the 3NiCo-CeZrO$_2$/S catalyst at T = 750 °C and a) 1.2 bar and b) 20 bar.

support's mobile lattice oxygen is one of very efficient pathways of carbon consumption towards the formation of CO.

In order to minimize metal cluster growth during the CH_4-CO_2 reforming reaction, several strategies have been utilized to date, for example employment of hexaaluminate [30], perovskite [31] and spinel [32] catalysts, which exhibit very high thermal stability and presence of atomically dispersed metals.

For stabilization of supported metal clusters and minimization of activity fluctuations during the reforming reaction, the second generation of catalysts was developed in which NiCo bimetallic and $CeZrO_2$ redox phases were anchored over the high surface area β-SiC; in the following text denoted as 3 NiCo-$CeZrO_2$/S. Fig. 7 shows TEM images of the 3NiCo-$CeZrO_2$/S catalyst prior to the catalytic reaction.

The material consists of crystalline SiC with clearly distinguishable lattice fringes of 0.26 nm, belonging to [111] SiC crystalline plane. SiC phase is encapsulated in a 5–8 nm thick amorphous SiO_2 layer (Fig. 7a), which indicates oxidation of the carbide phase during the catalyst calcination (12 h at 800 °C in air). NiCo bimetallic clusters were visualized as polydisperse polyhedral entities measuring on average 5.2 nm (Figs. 7b and 7c). Average NiCo cluster size was also analyzed also by H_2-TPD technique and found to measure 4.0 nm. This value is in good agreement with TEM data. $CeZrO_2$ phase was observed to be dispersed over the SiC support (EDXS elemental map) in the form of clusters, which were estimated to measure 8 nm size (Scherrer equation was applied to the most intensive reflection from the [111] crystalline plane of CeO_2, Fig. S5). Based on the results of H_2-TPR analysis, 39% of removable oxygen was quantified in $CeZrO_2$ redox support. This is considerably lower compared to the 3NiCo-$CeZrO_2$ catalyst (which does not contain β-SiC) and very likely occurs due to the anchoring and strong interaction with the non reducible amorphous SiO_2 layer, as observed during TEM analysis (Fig. 7).

The addition of a refractory support material (β-SiC) effectively spatially segregates the active phases as well as prevents their sintering, which results in stable catalyst activity (methane reforming rate of 0.18 mol/g_{cat} h) over extended time period of 550 h (Fig. 8a). No effect of catalyst deactivation/regeneration as described earlier (Fig. 5a) was observed in the case of 3NiCo-$CeZrO_2$/S catalyst. Further, only a minimal ill effect was observed due to lowering of the amount of redox promoter by 50%, as very low carbon yield was maintained: 7.4×10^{-4}% for 3NiCo-$CeZrO_2$/S catalyst during 550 h TOS vs. 8.9×10^{-5}% for 3NiCo/$CeZrO_2$ catalyst after 400 h TOS (Fig. 5a). It is interesting to note that carbon accumulation does not scale linearly with TOS (3NiCo/$CeZrO_2$ catalyst, 1×10^{-2}% at 30 h TOS), which indicates that carbon population of the catalyst's surface takes place in the initial stage of the reaction.

By considering results illustrated in Figs. 4a and 5a, we can conclude that NiCo bimetallic clusters below 45 nm in diameter, deposited over $CeZrO_2$ support with high extent labile oxygen, are key factors for low carbon accumulation and thus stable long term activity. On the other hand, large metal clusters (46 nm in diameter) with decreased metal-support interface will exhibit higher catalytic stability due to less oxygen spill over and lower partial oxidation of the metals. Considering these two opposing facts which favor either deactivation by coking or oxidation, the balance point exists in the introduction of SiC support which stabilizes the smaller NiCo clusters and simultaneously decreases the labile oxygen content in the $CeZrO_2$ redox promoter yielding stable catalytic activity (Fig. 8a).

In order to avoid extra energy (and cost) associated with compression stages, the methane reforming reaction is on the industrial scale performed at elevated pressures (20–80 bar). This, however, has at least three undesirable consequences: (i) lower achievable CH_4 and CO_2 conversion, (ii) carbon formation occurring under a significantly broader range of inlet feed compositions (gray line in the ternary diagram, Fig. 4b) [33] and (iii) the need for exotic materials and sophisticated reactor design. Due to these constraints, there are very few studies available in the open literature dealing with reforming reaction at elevated pressures [34–38]. Moreover, the reported results are rather pessimistic due to significantly enhanced rates of carbon deposition (compared to tests conducted at ambient pressure). As indicated by isotopically labeled reactants, a transition from CO_2 to CH_4 as the predominant source of deposited carbon takes place at elevated pressures [39].

The catalytic performance of 3NiCo-$CeZrO_2$/S catalyst developed in this work was studied in CH_4-CO_2 reforming reaction carried out at 20 bar total pressure. As can be seen in Fig. 8b, the produced syngas is considerably richer in CO (H_2/CO = 0.33, compared to 0.82 at 1.2 bar) as a result of more pronounced contribution of the RWGS reaction, which is also in accordance with theoretical calculations [33]. Stability of the catalyst is not an issue, as no noticeable decrease of CH_4 and CO_2 conversion can be observed when comparing values at 1 and 60 h TOS. The carbon yield at 20 bar pressure (8.8×10^{-3}% at 60 h TOS) is an order of magnitude higher compared to that obtained at 1.2 bar (7.4×10^{-4}% for 550 h TOS). This is a remarkable improvement (by 2–3 orders of magnitude) compared to the open literature reports, where considerably higher carbon yield values (0.34-1.94%) can be extracted from the experiments performed at very similar conditions [34,35]. These results confirm a harmonized role of active sites for CH_4 and CO_2 activation in the 3NiCo-$CeZrO_2$/S catalyst and indisputably constitute a promising basis for the design of a prospective technology for CO-rich syngas production through CH_4-CO_2 reforming reaction.

4. Conclusions

The 3NiCo/$CeZrO_2$ catalyst represents a promising basis for conversion of CH_4 and CO_2 to syngas with negligible coke accumulation within a wide range of CH_4:CO_2 feed compositions. At ambient pressure, the rate of carbon accumulation depends greatly on the metal cluster size and capability of the redox promoter for providing oxygen species to the metal clusters. To ensure low carbon yields over the catalyst, bimetallic NiCo clusters below 45 nm and $CeZrO_2$ mixed oxide with high extent labile oxygen have to be simultaneously present. By anchoring of the active catalytic phases over high specific surface area β-SiC (3NiCo-$CeZrO_2$/S catalyst), sintering and oxidation of bimetallic clusters can be significantly reduced, resulting in stable catalytic activity and low coke accumulation during test 550 h TOS.

During reforming conducted at 20 bar, lower CH_4 and CO_2 conversions were achieved due to thermodynamic restrictions, with syngas considerably richer in CO (H_2/CO = 0.33, compared to 0.82 at 1.2 bar, methane reforming rate of 0.18 mol/g_{cat} h). No catalyst deactivation was observed during 60 h of reaction at 20 bar. With the 3NiCo-$CeZrO_2$/S catalyst, accumulated carbon yields that are 2–3 orders of magnitude lower compared to state-of-the-art solids can be achieved, making it a highly promising candidate for possible industrial applications.

Appendix A. Supplementary data

Supplementary data associated with this article can be found, in the online version, at http://dx.doi.org/10.1016/j.apcatb.2017.01.064.

References

[1] PR Newswire, Syngas & Derivatives market, 2016. http://www.prnewswire.com/news-releases/syngas-and-derivatives-market-worth-213100-mw-thermal-by-2020-521372871.html (Accessed 18 April 2016).
[2] G. Yang, N. Tsubaki, J. Shamoto, Y. Yoneyama, Y. Zhang, J. Am. Chem. Soc. 132 (2010) 8129–8136.
[3] H.M. Torres Galvis, J.H. Bitter, C.B. Khare, M. Ruitenbeek, A.I. Dugulan, K.P. de Jong, Science 335 (2012) 835–838.
[4] E. Schwab, A. Milanov, S.A. Schunk, A. Behrens, N. Schödel, Chem. Ing. Tech. 87 (2015) 347–353.
[5] The state of renewable energies in Europe, 2013 edition; https://www.eurobserv-er.org/pdf/2013/EurObservER-Annual-Overview-2013-EN.pdf.
[6] M.A. Vasiliades, M.M. Makri, P. Djinović, B. Erjavec, A. Pintar, A.M. Efstathiou, Appl. Catal. B: Environ. 197 (2016) 168–183.
[7] A.S. Bobin, V.A. Sadykov, V.A. Rogov, N.V. Mezentseva, G.M. Alikina, E.M. Sadovskaya, T.S. Glazneva, N.N. Sazonova, M.Y. Smirnova, S.A. Veniaminov, C. Mirodatos, V. Galvita, G.B. Marin, Top. Catal. 56 (2013) 958–968.
[8] Z. Liu, D.C. Grinter, P.G. Lustemberg, T.-D. Nguyen-Phan, Y. Zhou, S. Luo, I. Waluyo, E.J. Crumlin, D.J. Stacchiola, J. Zhou, J. Carrasco, H.F. Busnengo, M.V. Ganduglia-Pirovano, S.D. Senanayake, J.A. Rodriguez, Angew. Chem. Int. Ed. 55 (2016) 7455–7459.
[9] J.K. Nørskov, T. Bligaard, J. Rossmeisl, C.H. Christensen, Nat. Chem. 1 (2009) 37–46.
[10] J. Zhang, H. Wang, A. Dalai, J. Catal. 249 (2007) 300–310.
[11] X. Chen, A. Tadd, J. Schwank, J. Catal. 251 (2007) 374–387.
[12] A. Gohier, C.P. Ewels, T.M. Minea, M.A. Djouadi, Carbon 46 (2008) 1331–1338.
[13] F. Besenbacher, I. Chorkendorff, B.S. Clausen, B. Hammer, A.M. Molenbroek, J.K. Nørskov, I. Stensgaard, Science 279 (1998) 1913–1915.
[14] H.S. Bengaard, J.K. Nørskov, J. Sehested, B.S. Clausen, L.P. Nielsen, A.M. Molenbroek, J.R. Rostrup-Nielsen, J. Catal. 209 (2002) 365–384.
[15] P. Fornasiero, G. Balducci, R. Di Monte, J. Kašpar, V. Sergo, G. Gubitosa, A. Ferrero, M. Graziani, J. Catal. 164 (1996) 173–183.
[16] B. Yan, X. Yang, S. Yao, J. Wan, M. Myint, E. Gomez, Z. Xie, S. Kattel, W. Xu, J.G. Chen, ACS Catal. 6 (2016) 7283–7292.
[17] P. Djinović, I.G. Osojnik Črnivec, B. Erjavec, A. Pintar, Appl. Catal. B 125 (2012) 259–270.
[18] M.M. Makri, M.A. Vasiliades, K.C. Petallidou, A.M. Efstathiou, Catal. Today 259 (2016) 150–164.
[19] M.-S. Fan, A.Z. Abdullah, S. Bhatia, Appl. Catal. B 100 (2010) 365–377.
[20] P. Djinović, I.G.O. Črnivec, A. Pintar, Catal. Today 253 (2015) 155–162.
[21] J. Zhang, H. Wang, A.K. Dalai, Appl. Catal. A: Gen. 339 (2008) 121–129.
[22] J.R. Rostrup-Nielsen, J. Catal. 85 (1984) 31–43.
[23] S. Tang, L. Ji, J. Lin, H.C. Zeng, K.L. Tan, K. Li, J. Catal. 194 (2000) 424–430.
[24] D.L. Trimm, Catal. Today 37 (1997) 233–238.
[25] M.S. Aw, I.G. Osojnik Črnivec, P. Djinović, A. Pintar, Int. J. Hydrogen Energy 39 (2014) 12636–12647.
[26] P. Djinović, I.G.O. Črnivec, B. Erjavec, A. Pintar, ChemCatChem 6 (2014) 1652–1663.
[27] K. Yuan, J.-Q. Zhong, X. Zhou, L. Xu, S.L. Bergman, K. Wu, G.Q. Xu, S.L. Bernasek, H.X. Li, W. Chen, ACS Catal. 6 (2016) 4330–4339.
[28] C.M. Kalamaras, S. Americanou, A.M. Efstathiou, J. Catal. 279 (2011) 287–300.
[29] C.M. Kalamaras, D.D. Dionysiou, A.M. Efstathiou, ACS Catal. 2 (2012) 2729–2742.
[30] T. Roussière, L. Schulz, K.M. Schelkle, G. Wasserschaff, A. Milanov, E. Schwab, O. Deutschmann, A. Jentys, J. Lercher, S.A. Schunk, ChemCatChem 6 (2014) 1438–1446.
[31] S.M. Lima, J.M. Assaf, M.A. Peña, J.L.G. Fierro, Appl. Catal. A: Gen. 311 (2006) 94–104.
[32] R. Lago, G. Bini, M.A. Peña, J.L.G. Fierro, J. Catal. 167 (1997) 198–209.
[33] R.Y. Chein, Y.C. Chen, C.T. Yu, J.N. Chung, J. Nat. Gas Sci. Eng. 26 (2015) 617–629.
[34] H.J. Ok, M.H. Park, D.J. Moon, J.H. Kim, N.C. Park, Y.C. Kim, J. Nanosci. Nanotechnol. 15 (2015) 449–453.
[35] B.K. Choi, Y.H. Park, D.J. Moon, N.C. Park, Y.C. Kim, J. Nanosci. Nanotechnol. 15 (2015) 5259–5263.
[36] L.C.S. Kahle, T. Roussière, L. Maier, K. Herrera Delgado, G. Wasserschaff, S.A. Schunk, O. Deutschmann, Ind. Eng. Chem. Res. 52 (2013) 11920–11930.
[37] K. Nagaoka, Y. Abe, Y. Hashimoto, T. Ishikawa, K. Sato, Y. Takita, T. Wakatsuki, M. Kunisu, E. Suda, S. Inamoto, ACS Catal. 3 (2013) 1564–1572.
[38] Y.-H. Wang, B.-Q. Xu, Catal. Lett. 99 (2005) 89–96.
[39] A. Shamsi, C.D. Johnson, Catal. Today 84 (2003) 17–25.
[40] D. Liu, R. Lau, A. Borgna, Y. Yang, Appl. Catal. A: Gen. 358 (2009) 110–118.
[41] D. Liu, X.Y. Quek, W.N.E. Cheo, R. Lau, A. Borgna, Y. Yang, J. Catal. 266 (2009) 380–390.
[42] X. Zhu, P. Huo, Y.P. Zhang, D.G. Cheng, C.J. Liu, Appl. Catal. B: Environ. 81 (2008) 132–140.